

Reactivity and Regioselectivity of Hydroxyl Radical Addition to Halogenated Ethenes

Sanja Sekušak,^{*,†} Klaus R. Liedl,[‡] and Aleksandar Sabljic^{†,§}

Department of Chemistry, Ruder Bošković Institute, P.O. Box 1016, HR-10001 Zagreb, Republic of Croatia, Institute of General, Inorganic and Theoretical Chemistry, University of Innsbruck, Innrain 52a, A-6020 Innsbruck, Austria, and Institut für Meteorologie und Klimaforschung, Forschungszentrum Karlsruhe/Universität Karlsruhe, D-76021 Karlsruhe, Germany

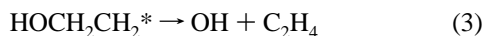
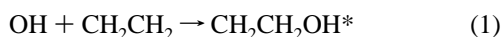
Received: July 28, 1997; In Final Form: November 6, 1997

The reactions of hydroxyl radical with ethene, fluoroethene, and chloroethene have been studied by quantum chemical methods. Reactants, prereaction complexes, transition-state structures, and products were optimized and vibrational frequencies were calculated at the UMP2/6-311+G(2d,p) level. Transition-state structures are significantly different from the prereaction complexes formed on the reactant side of the MEP. The convergence of barrier heights and reaction enthalpies has been systematically investigated with respect to the size and quality of basis set and the treatment of correlation energy. The best agreement with experimental results is found at the MP2/aug-cc-pVTZ level of theory. Regioselectivity is discussed in terms of two properties of the radical and the investigated alkenes. The first factor is the relative spin density in the $^3\pi\pi^*$ state of the alkene. The second factor is the relative strengths of the product C–O bond, i.e., relative stability of the corresponding radical product. In the case of fluoroethene these two effects oppose each other and regioselectivity is negligible. In the case of chloroethene spin density is the dominant factor and the addition of OH radicals to the unsubstituted carbon atom is preferred.

Introduction

The reaction of OH radical with ethene and halogenated ethene plays an important role in combustion kinetics¹ and atmospheric chemistry.^{2,3} Hydroxyl radicals attack alkenes by addition to the double bond to form hydroxy-substituted alkyl radicals, which then react with O₂ and follow the same general sequence as other alkyl radicals. The addition is typically the rate-limiting step in the degradation cycle. Thus, reaction rates with OH radicals determine the atmospheric lifetimes of all unsaturated hydrohalocarbons.⁴ From atmospheric lifetimes their global warming potential as well as their influence on stratospheric ozone depletion can be evaluated.⁵

Experimental studies on ethene reaction with OH radical² have shown that at temperatures below 450 K the predominant reaction mechanism is electrophilic addition of OH radicals to the π bond, forming an energy-rich HOCH₂CH₂* radical, which either can be collisionally stabilized or decomposes back into reactants:



At temperatures above 600 K hydrogen abstraction becomes the dominant pathway. A similar “low”- and “high”-temperature regime is found for the haloethene reactions with OH radicals. A small negative activation energy was found for all three reactions. Several explanations have been proposed for

such behavior including the formation of a weakly bound van der Waals complex.⁶

Radical addition to alkenes has been extensively investigated⁷ since it is a powerful synthetic means for formation of intermolecular bonds. It was found that such reactions are very difficult to describe well theoretically, and calculated barriers are found to be very sensitive to the level of theory employed.⁷ Regioselectivity of radical addition reactions to double bonds is still not well-understood. Several effects are apparently in competition, and the final result is difficult to predict. Additions to substituted ethenes proceed in two regiochemical pathways:⁸ the first “common” one is the attack on the less substituted carbon atom, and the “uncommon” one is the preferential addition to the more substituted end of the unsymmetric olefin.

Reactions of OH radical with ethene and haloethenes have been scarcely investigated theoretically.^{9,10} The reaction of OH radical with C₂H₄ has been studied at the PMP4(SDQ)/6-31G(d)//UHF/6-31G(d) level.⁹ Geometries of the van der Waals complex and transition-state structure were determined, and their harmonic frequencies were calculated. It was demonstrated that application of spin annihilation techniques and inclusion of electron correlation effects are crucial for obtaining results that are in agreement with experimental values. However, quite significant zero-point energy corrections were neglected and their inclusion would shift the calculated reaction barriers toward positive values. The reactions of OH radicals with monofluoroethene and 1,1'-difluoroethene have been studied recently,¹⁰ at the PMP4(SDQ)/6-311G(d,p)//UMP2/6-311G(d,p) level of theory, but structures of the van der Waals complex were not determined. To our knowledge, reaction of chloroethene with OH radical has not been studied yet.

The purpose of this work is a detailed study of reaction mechanisms and regioselectivity of ethene (R1), fluoroethene (R2), and chloroethene (R3) reactions with OH radicals:

* Corresponding author: Phone (385-1) 456-1089; Fax (385-1) 468-0084; E-mail: sanja@indigo.irb.hr.

† Ruder Bošković Institute.

‡ University of Innsbruck.

§ Universität Karlsruhe.



Barrier heights and reaction enthalpies have been calculated at a various levels of theory to identify the one most suitable for describing the addition of OH radicals to unsaturated hydrohalocarbons. The convergence of the calculated values with respect to the level of theory and the size of basis set employed is also investigated. Structures and energetics of reactants, van der Waals complexes, transition-state structures, and radical intermediates are determined. Factors influencing regioselectivity are examined and discussed.

Methods

Electronic Structure Calculations. The geometries of reactants, prereaction complexes, transition-state structures, and radical products were optimized and vibrational frequencies were calculated at the MP2(full)/6-311+G(2d,p) level of theory.¹¹ Minimum energy paths were calculated using the Gonzalez–Schlegel IRC algorithm at the same level of theory.¹² For the open-shell systems Schlegel’s spin projection scheme was used to eliminate spin contamination arising from states with spin ($s+1$) to ($s+4$).¹³ Vibrational frequencies were scaled with a scaling factor of 0.95, which has been derived from the study of Scott and Radom.¹⁴

Accurate total energies were calculated at the Gaussian-2 (G2) level of theory.¹⁵ Two modifications of original G2 theory were used: geometries were optimized and frequencies were calculated at the MP2/6-311+G(2d,p) level. Reaction barriers and enthalpies were also calculated at different levels of theory with correlated molecular orbital methods of different complexities and basis sets of different size. Pople’s double- and triple- ζ basis sets¹¹ augmented with polarization and diffuse functions as well as Dunning’s aug-cc-pVDZ and aug-cc-pVTZ basis sets¹⁶ were used. It was also of interest to apply density functional theory to the problem, and we have used the B3LYP method, i.e., Becke’s three-parameter hybrid method¹⁷ using the LYP correlation functional¹⁸ as implemented in the Gaussian94 program package.¹⁹ All energies were corrected by zero-point energies. For reaction enthalpies, thermal energies at 298 K were added. All calculations were carried out with the program package Gaussian94.¹⁹

The NBO analysis was performed with the NBO routine version 3.1,²⁰ which is integrated into the Gaussian94 suite of programs as link 607. The NBO method is discussed in detail by Weinhold et al.²¹ Semiquantitative and quantitative analyses of donor–acceptor interactions between various NBOs were made using the second-order perturbation theory ($\Delta E^{(2)}$) and the NBO Fock matrix deletion procedure.²² The deletion procedure is not self-consistent, but as long as the particular interactions in the Fock matrix, which have been zeroed, are not strongly coupled with other interactions, the error in energy is not significant.²³ Also, the energies are not strictly additive.²³ Fock matrices for α and β spin systems are deleted independently.²⁴ Simultaneous deletion of all off-diagonal Fock matrix elements results in the “Lewis energy” (E_{orb}) corresponding to a hypothetical molecule with strictly localized bonds. The energy difference between the total electronic energy and E_{orb}

TABLE 1: Experimental and Estimated Reaction Enthalpies of OH Radical Reactions with Ethene, Fluoroethene, and Chloroethene

ΔH_r°	method1 ^a	method2 ^a	expt
R1	−32.1	−29.5	−30.7 ± 0.9
R2a	−35.7	−31.8	
R3a	−38.1	−35.0	

^a As explained in the Methods section.

is labeled E_{orb^*} and represents much smaller effects of donor–acceptor delocalization away from perfectly localized Lewis structure. Thus, in our case, the interaction energy can be expressed as

$$\Delta E = E_{\text{transition-state}} - E_{\text{reactants}} = \Delta E_{\text{orb}} + \Delta E_{\text{orb}^*} \quad (1)$$

Experimental Results. The Arrhenius activation energy for ethene reaction with OH radicals was determined from the temperature dependence of the rate constant in the temperature range from 290 to 425 K and is equal to $-0.87 (\pm 0.09)$ kcal mol^{−1}. The reaction rate constant at 299 K and 98658 Pa is $(8.38 \pm 0.38) \times 10^{-12}$ cm³ molecule^{−1} s^{−1}. Rate constants for the fluoroethene and chloroethene reactions with OH radicals are available from a single study.² They were determined in the temperature range from 299 to 426 K. Arrhenius activation energies are calculated to be $-0.78 (\pm 0.30)$ and $-1.05 (\pm 0.30)$ kcal mol^{−1} for fluoroethene and chloroethene reactions with OH radicals, respectively. Rate constants at 298 K are 5.56×10^{-12} and 6.96×10^{-12} cm³ molecule^{−1} s^{−1} for fluoroethene and chloroethene reactions with OH radicals with an estimated uncertainty of 30%.

The experimental reaction enthalpy for the ethene reaction with OH radicals²⁵ is $\Delta H_r^\circ = -30.7 \pm 0.9$ kcal mol^{−1}. For the fluoroethene and chloroethene reactions with OH radicals there are no experimental values for reaction enthalpies. To calculate reaction enthalpies, enthalpies of formation of the hydroxyhaloalkyl radicals are needed. They can be estimated by using the group additivity model^{6c} (method1) or from the C–H bond dissociation energies of the corresponding alcohol (method2). Results are summarized in Table 1.

Using the group additivity model,^{6c} the heat of formation of the hydroxyethyl radical is -10.2 kcal mol^{−1}. Using this value, together with enthalpies of formation of the OH radical and ethene ($\Delta H_f^\circ(\text{OH}) = 9.4$ kcal mol^{−1}, $\Delta H_f^\circ(\text{C}_2\text{H}_4) = 12.5$ kcal mol^{−1})²⁶ the enthalpy of the ethene reaction with OH radicals is -32.1 kcal mol^{−1}, which is in very good agreement with the experimental value. The enthalpy of formation of the C₂H₄-OH radical can also be calculated from the enthalpy of formation of ethanol ($\Delta H_f^\circ(\text{C}_2\text{H}_5\text{OH}) = -56.1$ kcal mol^{−1})²⁷ and the hydrogen atom ($\Delta H_f^\circ(\text{H}) = 52.1$ kcal mol^{−1})²⁶ and from the C–H bond dissociation energy from the primary carbon atom in ethanol (method2). Since only the experimental value of the bond dissociation energy of the C–H bond from the secondary carbon atom in ethanol is available (~ 95.1 kcal mol^{−1}),²⁶ we used this value instead. The estimated enthalpy of formation for the C₂H₄OH radical is thus $\Delta H_f^\circ(\text{C}_2\text{H}_4\text{OH}) = -13.1$ kcal mol^{−1}. The reaction enthalpy calculated by using this value together with enthalpies of formation of the OH radical and ethene is -35.0 kcal mol^{−1}. C–H bond dissociation energy on the primary carbon atom in ethanol can also be approximated by the bond dissociation energy in ethane (100.7 ± 1.0 kcal mol^{−1}).²⁶ Then the estimated heat of formation of the C₂H₄-OH radical is -7.6 , giving the reaction enthalpy of $\Delta H_r^\circ = -29.5$ kcal mol^{−1}, which is in better agreement with experiment.

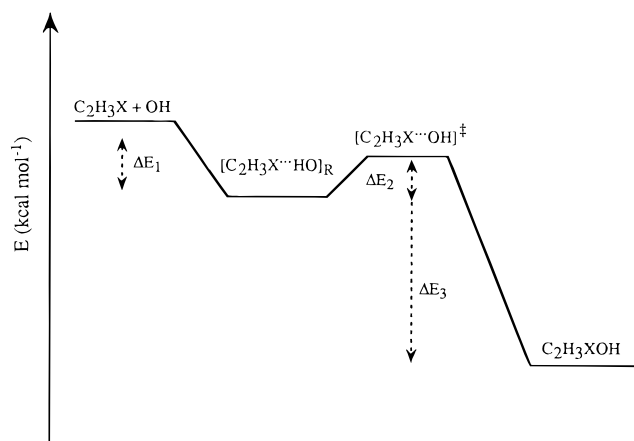


Figure 1. Potential energy diagram of ethene, fluoroethene, and chloroethene reactions with the OH radical.

Estimated by the group additivity model,^{6c} heats of formation of the α -hydroxyfluoroethyl and α -hydroxychloroethyl radicals are -57.9 and -23.7 kcal mol⁻¹, respectively. Using those values, together with heats of formation of fluoroethene ($\Delta H_f^\circ(\text{CH}_2\text{CHF}) = -31.6$ kcal mol⁻¹)^{6c} and the hydroxyl radical, gives reaction enthalpies of $\Delta H_r^\circ = -35.7$ kcal mol⁻¹ for reaction R2a and $\Delta H_r^\circ = -38.1$ kcal mol⁻¹ for reaction R3a. When the C–H bond dissociation energy in H–CH₂–CHFOH is approximated by the H–CH₂CH₂F bond dissociation energy²⁶ of 102 kcal mol⁻¹, the heat of formation of the α -hydroxyfluoroethyl radical is -54.0 kcal mol⁻¹. The enthalpy of fluoroethene reaction with the OH radical is thus $\Delta H_r^\circ = -31.8$ kcal mol⁻¹ using the value of the heat of formation of fluoroethanol ($\Delta H_f^\circ(\text{CH}_3\text{CHFOH}) = -103.9$ kcal mol⁻¹)^{6c} estimated with the group additivity model, the heat of formation of the hydrogen atom, fluoroethene ($\Delta H_f^\circ(\text{CH}_2\text{CHF}) = -31.6$ kcal mol⁻¹)^{6c} and the hydroxyl radical. The heat of formation of the α -hydroxychloroethyl radical is -20.8 kcal mol⁻¹ when approximate values for the C–H bond energy in chloroethane (101 kcal mol⁻¹)²⁶ and the enthalpy of formation of chloroethanol ($\Delta H_f^\circ(\text{CH}_3\text{CHClOH}) = -69.7$ kcal mol⁻¹)^{6c} are used. The estimated reaction enthalpy is $\Delta H_r^\circ = -35.0$ kcal mol⁻¹ using the heat of formation of chloroethene ($\Delta H_f^\circ(\text{CH}_2\text{CHCl}) = 5.0$ kcal mol⁻¹)^{6c} and the hydroxyl radical. For the β -addition reactions enthalpies were not estimated since enthalpies of formation for 2-fluoroethanol and 2-chloroethanol cannot be approximated using the bond additivity model.

Results

Rate constants for ethene (R1), fluoroethene (R2a, R2b), and chloroethene (R3a, R3b) reactions with OH radicals show negative temperature dependencies below 450 K. Therefore, negative activation energies are obtained in this region.² Negative values of activation energies have been explained by the formation of prereaction van der Waals complexes^{6c} with energies of the transition states lower than the energies of the reactant molecules. Figure 1 shows the energetic diagram of investigated radical reactions. The reaction paths for R1 and R2 reactions were investigated at the MP2(full)/6-311+G(2d,p) level of theory. Structures of reactants, van der Waals complexes, transition states, and radical products were determined. In the case of haloethene reactions with OH radicals only one structure of the van der Waals complex was found for both α - and β -addition, showing that the reaction bifurcates into two different reaction pathways once the reactant complexes are formed. Similar results were obtained for the α - and

β -pathways in H atom abstraction reactions of the OH radical with halogenated hydrocarbons.²⁸

A. Optimized Structures and Vibrational Frequencies.

1. Reactants and Products. Geometric parameters of the fully optimized reactant and product structures for reactions R1, R2, and R3 are given in Table 2. The calculated reactant geometries are in good agreement with experimental results.²⁹ Differences between the calculated and measured bond lengths are only a few thousandths of an angstrom, and the angles are reproduced within one degree. Calculated and measured³⁰ bond lengths of the hydroxyl radical are equal to 0.971 Å.

Geometries of the most stable conformers of the radical products in reactions R1, R2, and R3 are given in Table 3. The length of the newly formed C–O bond in the hydroxyethyl radical product is 1.429 Å. In the case of α -addition of the OH radical to the haloethenes the reactive C–O bond length is equal to 1.386 Å for the α -hydroxyfluoroethyl radical and 1.382 Å for the α -hydroxychloroethyl radical. In the case of β -addition, radical products show a C–O bond length similar to the CH₂CH₂OH radical, namely, 1.435 and 1.433 Å for reactions R'2b and R'3b. The bond between carbon atoms is approximately 0.04 Å shorter than the average single C–C bond and 0.15 Å longer than the average double bond. The orientation of the O–H bond with respect to the haloethene is determined by the electron densities on the radical carbon atoms and on the halogen atom. Other conformations are shown in Figure 2, and the relative stabilities of conformers are shown in Table 3. All conformers are very close in energy.

Harmonic vibrational frequencies for reactants and products are given in Tables 4 and 5. Frequencies are scaled by factor 0.95.³¹ The frequency scaling reduces the rms error from 115 to 108 cm⁻¹ for ethene, from 57 to 13 cm⁻¹ for fluoroethene, and from 63 to 14 cm⁻¹ for chloroethene. The calculated O–H stretching frequency for the hydroxyl radical is 3797 cm⁻¹, which is in very good agreement with the experimental value of 3738 cm⁻¹.³² The scaled value is 3607 cm⁻¹.

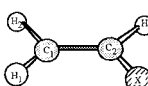
Fluorine substitution increases the C=C vibrational frequency and decreases the torsion frequency in ethene. This indicates that the strength of the σ bond is increased and the strength of the π bond is decreased. In the case of chloroethene both the C=C stretching and the torsion frequency are reduced. Substitution of the hydrogen atom by a halogen atom causes, in terms of the frontier orbital approach, a mixing of the halogen lone pairs with the HOMO molecular orbital in an antibonding fashion (see Figure 3). Also, charge polarization in the fluoroethane molecule results in a stronger σ bond. The net effect of the halogen atom substitution on ethene is a result of the resonance and inductive effects, which leads to the stabilization of the HOMO orbital in fluoroethene and destabilization in chloroethene.

The analysis of normal modes shows that the stretching frequency of the newly formed C–O bond is coupled with the C–C stretching frequency ($\nu(\text{CC})-\nu(\text{CO})$). It is equal to 1052 cm⁻¹ for the CH₂CH₂OH radical. For the CH₂CHFOH and CHFCH₂OH radicals, the $\nu(\text{CC})-\nu(\text{CO})$ frequency increases in comparison to the CH₂CH₂OH radical. They rise to 1109 and 1122 cm⁻¹, respectively. In the case of the reactions R3a and R3b $\nu(\text{CC})-\nu(\text{CO})$ frequencies are lower than for the CH₂CH₂OH radical and equal to 872 and 1068 cm⁻¹ for the CH₂CHClOH and CHClCH₂OH radicals.

2. van der Waals Complexes and Transition-State Structures.

Geometries of prereaction van der Waals complexes and transition-state structures are given in Table 1. The main difference between van der Waals complexes and transition-

TABLE 2: Geometric Parameters for Reactants, Prereaction Complexes, Transition-state Structures, and Radical Products for Ethene (R1), Fluoroethene (R2), and Chloroethene (R3) Reactions with the OH Radical Calculated at the MP2/6-311+G(2d,p) Level of Theory (Bond Lengths in Å and Angles in deg)

Parameters	R1	R2	R3
Reactants			
 r(C1-C2)	1.333 (1.339) ^a	1.323 (1.329)	1.327 (1.333)
r(C1-H1)	1.083 (1.085)	1.081 (1.087)	1.082 (1.089)
r(C1-H2)	1.083 (1.085)	1.080 (1.077)	1.083 (1.070)
r(C2-H3)	1.083 (1.085)	1.082 (1.082)	1.082 (1.080)
r(C2-X)	1.083 (1.085)	1.349 (1.347)	1.738 (1.726)
θ(H1-C1-H2)	117.2 (117.8)	119.8 (120.1)	118.9 (118.4)
θ(H1-C1-C2)	121.4	121.3 (120.9)	121.9 (121.0)
θ(H3-C2-X)	117.2	112.1 (110.0)	113.4 (114.3)
θ(C1-C2-X)	121.4	121.9 (120.8)	123.2 (122.7)
Symmetry	(C _s)	(C _s)	(C _s)
Pre-reaction complexes			
r(C1-C2)	1.336	1.326	1.331
r(C1-H1)	1.084	1.082	1.083
r(C1-H2)	1.084	1.081	1.083
r(C2-H3)	1.084	1.083	1.083
r(C2-X)	1.084	1.345	1.740
r(H4-C1)	2.487	2.478	2.555
r(H4-C2)	2.487	2.586	2.555
θ(H1-C1-H2)	117.2	119.9	119.9
θ(H1-C1-C2)	121.4	121.3	121.3
θ(H3-C2-X)	117.2	112.3	112.3
θ(C1-C2-X)	121.4	121.7	123.0
φ(H3-C2-C1-X)	180.5	179.8	179.8
φ(H1-C1-C2-H2)	179.5	181.6	181.6
φ(O-H4-C1-C2)	0.0	157.6	159.3
Transition-state structures			
(α-addition)			
r(C1-C2)	1.333	1.324	1.326
r(C1-H1)	1.081	1.081	1.081
r(C1-H2)	1.081	1.078	1.080
r(C2-H3)	1.083	1.080	1.079
r(C2-X)	1.083	1.333	1.735
r(O-C2)	2.067	2.045	2.018
θ(H1-C1-H2)	117.0	120.2	119.2
θ(H1-C1-C2)	121.0	120.7	119.2
θ(H3-C2-X)	117.6	112.8	113.3
θ(C1-C2-X)	121.2	121.1	122.0
θ(C1-C2-O)	97.4	92.8	92.3
φ(H3-C2-C1-X)	167.9	167.4	165.0
φ(H1-C1-C2-H2)	178.0	178.4	177.5
φ(H4-O-C1-C2)	13.9	47.0	52.6
(β-addition)			
r(C1-C2)		1.322	1.322
r(C1-H1)		1.078	1.080
r(C1-H2)		1.080	1.080
r(C2-H3)		1.081	1.080
r(C2-X)		1.345	1.734
r(O-C1)		2.048	2.059
θ(H1-C1-H2)		119.1	118.3
θ(H1-C1-C2)		118.3	121.6
θ(H3-C2-X)		112.5	113.7
θ(C1-C2-X)		121.6	122.9
θ(C1-C2-O)		98.8	97.9
φ(H3-C2-C1-X)		184.1	183.6
φ(H1-C1-C2-H2)		165.0	166.7
φ(H4-O-C1-C2)		42.1	36.9
Products			
(α-addition)			
r(C1-C2)	1.483	1.482	1.467
r(C1-H1)	1.081	1.079	1.079
r(C1-H2)	1.080	1.079	1.081
r(C2-H3)	1.095	1.092	1.086
r(C2-X)	1.095	1.397	1.862
r(O-C2)	1.429	1.386	1.382
r(O-H4)	0.965	0.966	0.967
θ(H1-C1-H2)	118.8	120.2	119.0
θ(H1-C1-C2)	119.2	118.9	119.7
θ(H3-C2-X)	107.0	106.0	103.4
θ(C1-C2-X)	110.4	107.9	107.1
θ(C2-O-H4)	107.2	107.1	108.7
φ(H3-C2-C1-X)	118.5	117.1	113.3
φ(H1-C1-C2-H2)	167.2	167.6	163.9
φ(H1-C1-C2-O)	153.5	151.3	167.7
φ(H4-O-C2-C1)	54.4	47.1	52.7
(β-addition)			
r(C1-C2)		1.476	1.481
r(C1-H1)		1.094	1.094
r(C1-H2)		1.089	1.090
r(C2-H3)		1.082	1.080
r(C2-X)		1.355	1.721
r(O-C1)		1.435	1.433
r(O-H4)		0.965	0.966
θ(H1-C1-H2)		108.6	108.6
θ(H1-C1-C2)		109.8	110.1
θ(H3-C2-X)		112.5	114.6
θ(C1-C2-X)		114.2	117.7
θ(C2-O-H4)		107.5	107.4
φ(H3-C2-C1-X)		143.3	153.4
φ(H1-C1-C2-H2)		119.0	119.2
φ(H3-C2-C1-O)		72.4	78.5
φ(H4-O-C1-C2)		92.2	61.9

^a Ref 29.

TABLE 3: Relative Stabilities (kcal mol⁻¹) of Conformers for Radical Products in Ethene, Fluoroethene, and Chloroethene Reactions with the OH Radical Calculated at the MP2/6-311+G(2d,p) Level

radical	I	II	III	<i>E</i> _{min} ^a
R1	0.0			-154.070 417
R2				
α-addition	0.0			-253.207 649
β-addition	1.1	0.9	0.0	-253.193 748
R3				
α-addition		0.0	1.2	-613.216 673
β-addition	0.8	0.7	0.0	-613.213 199

^a Total energies (hartrees) for the lowest energy conformer of each radical.

state structures is the orientation of the OH radical with respect to the hydrocarbon molecule. In the van der Waals complexes the hydroxyl radical is oriented perpendicular to the hydrocarbon plane, forming a weak hydrogen bond between the hydrogen atom of the OH radical and the π electron density of the double bond. In the transition-state structures the oxygen atom of the OH radical is rotated toward the carbon atom in order to form the new C2–O bond.

The van der Waals complex formed in the ethene reaction with the OH radical has C_s symmetry, with r(C1–H4) and r(C2–H4) distances of 2.487 Å. The r(C1–H4) and r(C2–H4) distances are also the same in the case of chloroethene reaction with the OH radical and equals 2.555 Å. In the case of the fluoroethene reaction with the OH radical the H4 atom is closer to the unsubstituted, i.e., β-carbon atom, (2.478 Å) than to the substituted carbon atom (2.586 Å). Geometries of the reactants are only slightly perturbed in the van der Waals complexes, preserving the ethene molecule's planarity, while the carbon atoms in fluoroethene and in chloroethene are slightly rehybridized. Interactions between the reactants in the van der Waals structures are well-characterized by π electron density delocalization into the antibonding σ*(OH) orbital of the hydroxyl radical. Details of the NBO analysis are given later in the text.

The geometric parameters for the transition-state structures are given in Table 2. All transition-state structures are reactantlike with mainly conserved character of the double bond between carbon atoms and planarity of the π system. The unpaired electron is still centered at the oxygen atom. The distance between the carbon and oxygen atom is 2.067 Å for reaction R1, 2.045 Å for reaction R2a, and 2.018 Å for reaction R3a. In the case of β-addition, the C–O distance is 2.048 Å in the transition-state structure for reaction R2b and 2.059 Å for reaction R3b. The orientation of the O–H bond with respect to the hydrocarbon molecule is imposed by the π electron density of the C–C bond and the position of the halogen atom. The rotational potential of O–H internal rotation around the partially formed C–O bond is 2-fold and asymmetric. Rotational barriers and corresponding vibrational frequencies are given in Table 6.

Vibrational frequencies of the van der Waals complexes are given in Table 7. The lowest vibrational frequency of the vdW complex between ethene and OH, ν₁ = 80 cm⁻¹, becomes the reaction coordinate for the addition reaction. The corresponding normal mode vector is given in Figure 4. For the fluoroethene and chloroethene vdW complexes the ν₁ frequencies are 69 and 72 cm⁻¹. The vibrational frequency ν₃ corresponds to the reaction coordinate for the formation (and decomposition) of the vdW complex from reactant molecules.

All transition-state structures have one negative eigenvalue of the Hessian. The calculated vibrational frequencies are given

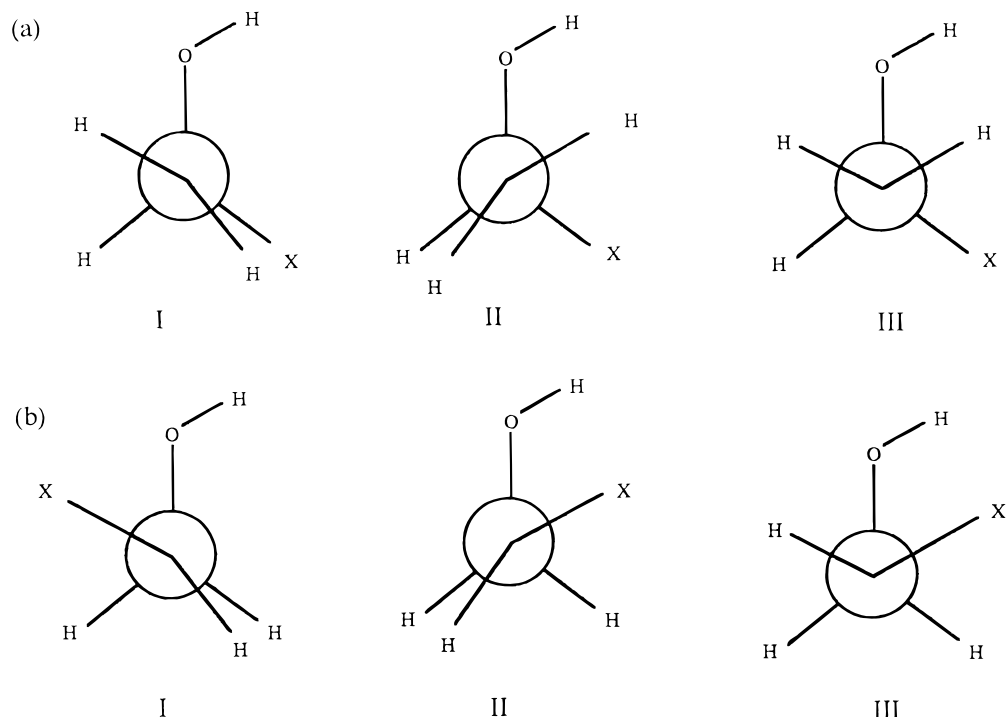


Figure 2. Newman projections representing the conformations of the lowest energy radical products of (a) α -addition and (b) β -addition of the OH radical on ethene (X = H) and haloethenes (X = F, Cl).

TABLE 4: Harmonic Vibrational Frequencies (cm^{-1}) of Ethene, Fluoroethene, and Chloroethene

ethene					fluoroethene					chloroethene			
sym	dominant normal modes ^a	MP2/6-311+G(2d,p)	scal ^b	expt ^c	sym	dominant normal modes ^a	MP2/6-311+G(2d,p)	scal	expt ^d	sym	MP2/6-311+G(2d,p)	scal	expt ^e
A _g	$\nu(\text{CH}_2)_s$	3185	3026	3019	A'	$\nu(\text{CH}_2)_a$	3315	3149	3150	A'	3293	3128	3121
A _g	$\nu(\text{CC})$	1679	1595	1623	A'	$\nu(\text{CH})$	3247	3085	3115	A'	3244	3082	3086
A _g	$\delta(\text{CH}_2)$	1383	1314	1342	A'	$\nu(\text{CH}_2)_s$	3204	3044	3080	A'	3187	3028	3030
B _{1g}	$\nu(\text{CH}_2)_a$	3283	3119	3273	A'	$\nu(\text{CC})$	1702	1617	1654	A'	1656	1573	1608
B _{1g}	$\rho(\text{CH}_2)$	1246	1184	1050	A'	$\delta(\text{CH}_2)$	1428	1357	1380	A'	1424	1353	1369
B _{2g}	$\Gamma(\text{CH}_2)_a$	936	889	943	A'	$\delta(\text{CH}_2)$	1340	1273	1306	A'	1309	1244	1279
A _u	$\tau(\text{CH}_2)$	1064	1011	995	A'	$\nu(\text{CX})$	1168	1110	1156	A'	1052	999	1030
B _{1u}	$\Gamma(\text{CH}_2)_s$	971	922	949	A'	$\rho(\text{CH}_2)$	938	891	929	A'	903	858	896
B _{2u}	$\nu(\text{CH}_2)_a$	3258	3095	3105	A'	$\rho(\text{CH}_2)$	484	460	483	A'	400	380	395
B _{2u}	$\rho(\text{CH}_2)$	835	793	825	A''	$\tau(\text{CH}_2)$	960	912	940	A''	980	931	941
B _{3u}	$\nu(\text{CH}_2)_s$	3168	3010	2989	A''	$\Gamma(\text{CH}_2)$	860	817	863	A''	735	698	720
B _{3u}	$\delta(\text{CH}_2)$	1494	1419	1443	A''	$\Gamma(\text{CH}_2)$	731	694	711	A''	637	605	620

^a ν , stretch; δ , bend; ρ , rock; Γ , pyramidal distortion; τ , torsion. ^b Values are scaled by 0.95. Ref 31. ^c Ref 32a. ^d Ref 32b. ^e Ref 32c.

TABLE 5: Harmonic Vibrational Frequencies of Radical Products in Ethene, Fluoroethene, and Chloroethene Reactions with the OH Radical Calculated at the MP2/6-311+G(2d,p) Level

product	frequencies (cm^{-1}) ^a
CH ₂ CH ₂ OH	3646 3151 3038 2936 2898 1445 1417 1348 1309 1139 1083 1052 915 802 514 409 319 184
CH ₂ CHFOH	3622 3175 3055 2956 1415 1374 1307 1225 1109 1052 940 845 602 503 447 398 360 147
CHFCH ₂ OH	3649 3082 3000 2864 1435 1368 1320 1303 1183 1122 1018 967 847 664 452 322 262 122
CH ₂ CHClOH	3622 3160 3043 3025 1424 1369 1264 1179 1119 1025 872 633 548 459 402 307 279 185
CHClCH ₂ OH	3641 3107 2953 2901 1437 1353 1302 1260 1154 1068 972 934 720 542 344 285 238 92

^a Values are scaled by 0.95.

in Table 8. The eigenvector that corresponds to the imaginary frequency is shown in Figure 4b for reaction R1 and is primarily a translation of the OH radical toward the hydrocarbon molecule that becomes the C–O stretching frequency in the radical products. The same situation happens in the case of OH addition

to haloethenes. The lowest real vibrational frequency in the transition-state structure for reaction R1, ν_2 , corresponds to the hindered rotation of the hydroxyl hydrogen atom around the C–O bond. For the transition-state structures of the α -addition of an OH radical to halocarbons this frequency is somewhat higher (ν_2 for R2a and ν_3 for R3a) because of the additional interaction of the hydrogen and halogen atoms (Table 6). In the case of β -addition the hindered rotation frequencies are even higher (ν_3 for both R2b and R3b reactions).

The ability of density functional theory to describe OH radical addition reactions was tested using the B3LYP/6-311+G(2d,p) method. Transition-state structures optimized at the DFT level are quite different from the structures obtained with the MP2 method. For the OH radical addition to ethene the DFT structure has C_s symmetry with the OH group equally distant from both carbon atoms and oriented perpendicular to the C–C bond. The distance between the oxygen atom and the center of the double bond is found to be 2.3108 Å, while MP2 optimization yields 2.1680 Å. For the OH addition to fluoroethene only one transition-state structure was determined for both α - and

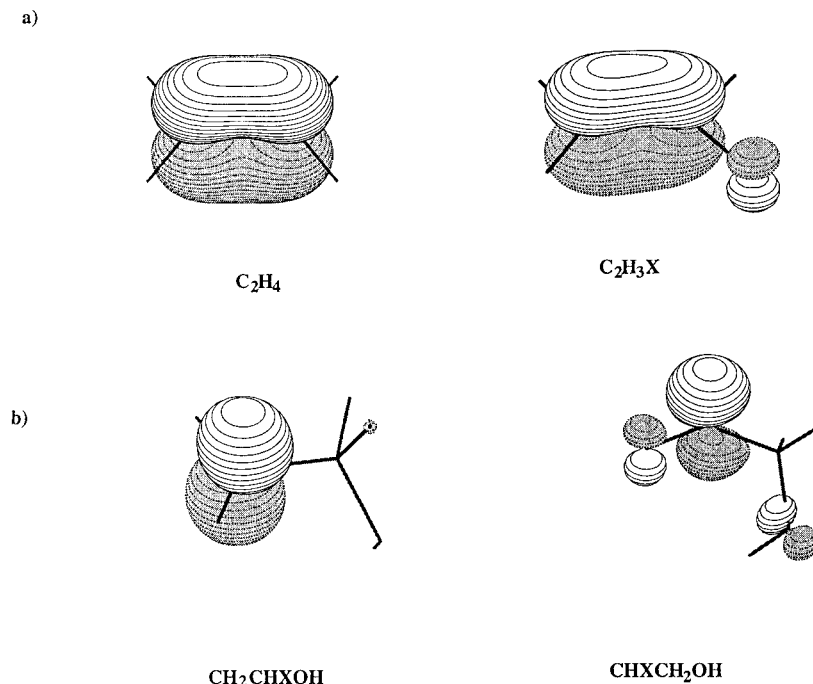


Figure 3. HOMO orbitals of (a) reactants and (b) products of OH radical reaction with ethene and haloethenes.

TABLE 6: Vibrational Frequencies (cm^{-1}) and Energy Barriers for Internal Rotation ($kcal\ mol^{-1}$) of the Hydrogen Atom of the OH Radical around the Reactive C–O Bond Calculated at the UMP2/6-311+G(2d,p) Level of Theory

transition state	frequency	$E_{rot}(1)$	$E_{rot}(2)$
$[CH_2CH_2\cdots OH]$	112	0.05	4.36
$[CH_2CHF\cdots OH]$	161	0.33	4.53
$[CHFCH_2\cdots OH]$	176	0.54	3.35
$[CH_2CHCl\cdots OH]$	154	0.95	4.58
$[CHClCH_2\cdots OH]$	170	0.51	3.69

β -addition, in which the OH radical is positioned symmetrically with respect to both carbon atoms. The reactive C–O distances are about 0.5 Å longer than in the case of MP2 results, and the O–H bond is oriented perpendicular to the C–C double bond. In the case of the chloroethene reaction with the OH radical two different transition-state structures are found, one for α - and one for β -addition with C–O distances also about 0.5 Å longer in comparison to the MP2 results. The orientation of the O–H bond with respect to halocarbon moiety is not sensitive to the position of the halogen atom since there is no attractive interactions between the O–H radical and halogen atom from the halocarbon molecule. Therefore, the O–H bond is positioned on the other side of the C–C double bond from the halogen atom.

B. Reaction Enthalpies and Barrier Heights. The reaction enthalpies and barrier heights are found to be very sensitive to the level of theory employed. Both quantities are corrected for the zero-point energy difference, and reaction enthalpies are corrected for thermal energy calculated at 298 K. Results are given in Tables 8 and 9. The spin contamination of the unrestricted wave function of the van der Waals complexes,

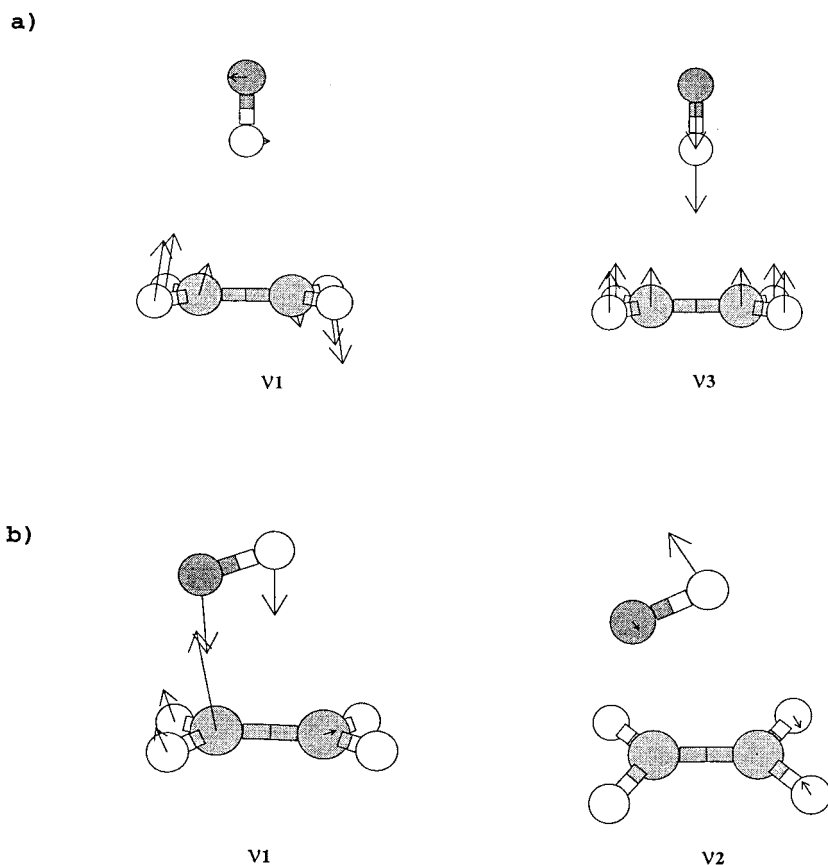
transition-state structures, and radical products is relatively small, but still it has a noticeable effect on the calculated barrier heights. The largest spin contamination is obtained for the transition-state structures with the expectation value of the S^2 operator never larger than 0.9. Projecting out the spin contamination lowers the MP2 and MP4 barrier heights by 6–7 $kcal\ mol^{-1}$ and the reaction enthalpies by approximately 3 $kcal\ mol^{-1}$, improving their agreement with experimental data. Thus, the annihilation of the spin contamination from the unrestricted wave functions seems to be mandatory for calculation of both reaction enthalpies and barrier heights. This result is in agreement with results of previous investigations of radical reactions.^{7,9,10,33}

For smaller basis sets, the calculated barrier heights are in slight agreement with Arrhenius activation energies calculated from experiment. The increase of the basis set size, especially the addition of diffuse and polarization functions, decreases deviations from experimental data. The best agreement between theoretical and experimental results is obtained using the Dunning's aug-cc-pVTZ basis set at the MP2 level. The difference between MP2 and MP4 barrier heights is, on average, 0.5 $kcal\ mol^{-1}$. Interestingly, quite reliable results are obtained at the MP2/6-311+G(2d,p) level of theory, with deviations from activation energies being less than 1 $kcal\ mol^{-1}$. Gaussian-2 theory fails to describe the investigated reactions as a consequence of the inferior results obtained by the MP2, MP4, and QCISD(T) methods in combination with small basis sets such as 6-311G(d,p) and 6-311+G(d,p) that are used within the G2 scheme. Therefore, the G2 method is not suitable for the prediction of energetics of OH addition to ethene and halogenated analogues, in contrast to the very good results obtained for abstraction reactions.³³ The best results are obtained using the MP2 method with large basis sets, such as 6-311+G(3df,2p), 6-311++G(3df,2pd), aug-cc-pVDZ, and aug-cc-pVTZ, which are in agreement with measured reactivity.

Barrier heights calculated also at the CCSD(T)/6-311+G(2d,p) level ($\Delta E_0^\ddagger(\text{ethene}) = 2.6$ and $\Delta E_0^\ddagger(\text{fluoroethene}) = 2.1$ $kcal\ mol^{-1}$) are in faint agreement with experiment. Obviously

TABLE 7: Harmonic Vibrational Frequencies for van der Waals (vdW) Complexes in Ethene, Fluoroethene, and Chloroethene Reactions with the OH Radical Calculated at the MP2/6-311+G(2d,p) Level

vdW complex	frequencies (cm ⁻¹) ^a
[CH ₂ CH ₂ ⋯HO] symmetry C _s	3536 3022 3009 1592 1420 1313 940 906 356 104 76 3119 3094 1184 1020 793 298 89 A' A' A' A' A' A' A' A' A' A' A'' A'' A'' A'' A'' A'' A''
[CH ₂ CHF⋯HO] symmetry C _i	3552 3145 3083 3039 1617 1358 1274 1115 924 895 830 712 461 324 238 95 66 30
[CH ₂ CHCl⋯HO] symmetry C _i	3563 3122 3076 3020 1583 1352 1244 998 937 866 696 623 385 339 232 89 68 26

^a Values scaled by 0.95.**Figure 4.** Normal modes for some vibrational frequencies of the (a) prereaction complex and (b) the transition-state structure of ethene reaction with the OH radical.**TABLE 8: Harmonic Vibrational Frequencies for Transition-State Structures in Ethene, Fluoroethene, and Chloroethene Reactions with the OH Radical**

transition state	frequencies (cm ⁻¹) ^a
[CH ₂ CH ₂ ⋯OH]	3582 3147 3118 3048 3026 1596 1431 1316 1200 1068 1024 955 808 715 408 218 112 491i
[CH ₂ CFH⋯OH]	3591 3171 3116 3057 1616 1368 1278 1143 1024 916 884 716 692 479 289 211 161 555i
[CFHCH ₂ ⋯OH]	3601 3170 3105 3065 1611 1364 1282 1117 994 953 901 821 734 468 262 176 116 558i
[CH ₂ CClH⋯OH]	3591 3154 3117 3045 1568 1364 1241 1042 1005 923 761 698 630 398 278 190 155 617i
[CClHCH ₂ ⋯OH]	3601 3158 3105 3057 1581 1354 1256 1022 1006 971 749 732 698 390 257 170 110 531i

^a Values scaled by 0.95

for such a sophisticated method larger basis sets are needed in order to obtain satisfactory results.

Reaction enthalpies calculated at different levels of theory for ethene, fluoroethene, and chloroethene reactions with the OH radical are given in Table 10. The reaction enthalpy was measured only for the ethene reaction with the OH radical, while reaction enthalpies for fluoroethene and chloroethene reactions

with the OH radical were only estimated as explained in the Methods section. The values calculated in this paper should be more reliable than these estimates. Good agreement with experiment is obtained for the MP2 method with aug-cc-pVDT, aug-cc-pVTZ, 6-311++G(3df,2p), and 6-311+G(2df,2p) basis sets in analogy with the calculated barrier heights. Again, agreement within the experimental error is obtained with a moderately sized 6-311(2d,p) basis set. As in the case of the barrier heights, MP2 results are in better agreement with experiment than the MP4 results; typical differences between the two methods are 2–3 kcal mol⁻¹.

The energetic diagrams for all investigated reactions were calculated at several levels of theory. The results obtained at the MP2/aug-cc-pVTZ level are given in Table 12. Energy differences given in Table 12 are explained in Figure 1. The most stable vdW π complex is formed in the ethene reaction, whereas the one formed between fluoroethene and the OH radical is the least stable in the investigated series. Calculated stabilization energies are in agreement with the NBO analysis, whose results are described in the following section.

Basis set superposition errors were calculated for the series of basis sets used in the investigations of R1 and R2a reactions.

TABLE 9: Barrier Heights of Ethene, Fluoroethene, and Chloroethene Reactions with the OH Radical Calculated at Different Levels of Theory (kcal mol⁻¹)

method ^a		ΔE_0^\ddagger				
		ethene + OH (R1)	fluoroethene + OH (R1a) (R2b)		chloroethene + OH (R3a) (R3b)	
6-311+G(2d,p)	B3LYP	-2.90	-3.5		-2.1	-1.5
6-311+G(2d,p)	PMP2	0.06	0.50	0.43	1.85	0.03
6-311G(d,p)	PMP2	2.53	2.42	2.99		
	PMP4	3.10	3.02	3.40		
	QCISD(T)	4.53	3.80	4.30		
6-311+G(d,p)	PMP2	1.80	2.32	2.37		
	PMP4	2.10	2.64	2.49		
6-311G(2df,p)	PMP2	0.62	0.25	1.00		
	PMP4	1.16	0.85	1.40		
6-311+G(3df,2p)	PMP2	-0.32	-0.08	0.17	1.11	-0.46
6-311++G(3df,3pd)	PMP2	-0.27	-0.06	0.22		
aug-cc-pVDZ	PMP2	-0.32	0.09	0.17	1.06	-0.31
aug-cc-pVTZ	PMP2	-0.69	-0.34	-0.15	0.98	-0.63
G2		1.39	0.99	1.16		
expt		-0.87 ± 0.09	-0.77 ± 0.30		-1.05 ± 0.30	

^a Equilibrium geometries and vibrational frequencies are calculated at the MP2/6-311+(2d,p) level except for the B3LYP results.

TABLE 10: Enthalpies of Ethene, Fluoroethene, and Chloroethene Reactions with the OH Radical Calculated at Different Levels of Theory (kcal mol⁻¹)

method ^a		ΔH_r^{298}				
		ethene + OH (R1)	fluoroethene + OH (R2a) (R2b)		chloroethene + OH (R3a) (R3b)	
6-311+G(2d,p)	B3LYP	-25.4	-33.4	-26.3	-31.4	-27.8
6-311+G(2d,p)	PMP2	-30.5	-38.5	-30.3	-34.3	-31.3
6-311G(d,p)	PMP2	-30.0	-38.5	-29.4		
	PMP4	-29.2	-34.8	-26.1		
	QCISD(T)	-25.4	-33.8	-25.5		
6-311+G(d,p)	PMP2	-30.1	-37.9	-29.8		
	PMP4	-26.7	-34.4	-26.6		
6-311G(2df,p)	PMP2	-31.9	-40.1			
	PMP4	-27.7	-36.0			
6-311+G(3df,2p)	PMP2	-32.7	-40.8	-30.4	-35.8	-34.0
6-311++G(3df,3pd)	PMP2	-32.1	-40.6	-30.4	-36.8	
aug-cc-pVDZ	PMP2	-31.0	-39.5	-29.1	-35.9	-32.1
aug-cc-pVTZ	PMP2	-32.2	-40.1	-29.9	-36.1	-33.5
G2		-27.2	-35.9	-30.1		
expt		(-30.7 ± 0.9)	≈(-31.8)-(-35.7)		≈(-35.0)-(-38.1)	

^a Equilibrium geometries and vibrational frequencies are calculated at the MP2/6-311+(2d,p) level.

TABLE 11: Stabilization Energies of the van der Waals Complexes with Respect to the Reactants for the Different Levels of Theory. Values Are Zero-Point-Corrected and Given in kcal mol⁻¹

method	reactions		
	R1	R2	R3
B3LYP/6-311+G(2d,p)// B3LYP/6-311+G(2d,p)	-1.40	-0.98	-0.97
MP2/6-311+G(3df,2p)// MP2/6-311+G(2d,p)	-2.01	-1.52	-1.70
MP2/aug-cc-pVTZ// MP2/6-311+G(2d,p)	-2.04	-1.58	-1.68

For the van der Waals complexes the calculated BSSEs are much smaller than for transition-state structures. In the case of ethene reaction the BSSE calculated at the MP2/6-311+G(2d,p) level is 0.64 kcal mol⁻¹ for the vdW complex and 1.17 kcal mol⁻¹ for the transition-state structure. Increasing the basis set size increases the value of the BSSE. For MP2/6-311++G(3df,2pd) and aug-cc-pVDZ basis sets the BSSE is 1.20 and 1.82 kcal mol⁻¹. This is in agreement with well-known nonmonotonic behavior of the BSSE.³⁴ For the fluoroethene reaction with the OH radical the BSSE is somewhat larger than that in the case of ethene due to the smaller reactive C–O distance in the transition-state structures and the delocalization of the lone-

TABLE 12: Reaction Energetics for Ethene (R1), Fluoroethene (R2), and Chloroethene (R3) Reactions with the OH Radical Calculated at the MP2/aug-cc-pVTZ Level. Values Are Zero-Point-Corrected and Given in kcal mol⁻¹. Reaction Enthalpies Are Additionally Corrected for Thermal Energies Calculated at 298 K and for the ΔpV Term

reaction	ΔE_1	ΔE_2	ΔE_3	ΔE_0^\ddagger	ΔH_r^{298}
R1	-2.04	1.35	-29.74	-0.69	-32.23
R2a	-1.58	1.29	-38.70	-0.34	-40.15
R2b		1.49	-28.70	-0.15	-29.93
R3a	-1.68	2.66	-36.07	0.98	-36.10
R3b		1.96	-31.73	-0.63	-33.35

pair electron density from fluorine into the partial C–O bond. Values of the BSSE are 2.64 and 1.87 kcal mol⁻¹ for reaction R1a at the MP2/6-311+G(2d,p) and MP2/6-311++G(3df,2pd) levels. From these calculations it is obvious that the values of the BSSE do not converge within the size of the basis sets employed. Also, correction of the barrier height values for the calculated BSSE drastically deteriorates agreement with experiment. Similar results are already obtained from recent high level calculations on the dimmers of hydrogen fluoride,³⁵ water,³⁶ and carbonic acid.³⁷ The value of the BSSE is not calculated at MP2/aug-cc-pVTZ because of the SCF convergence problems.

TABLE 13: Natural Bond Orbital Charge-Transfer Analysis of the Calculated Transition-State Structures at the UHF/6-311+G(2d,p)//UMP2/6-311+G(2d,p) Level of Theory^a

TS (A···B)	ΔE	$\Delta E_{CT}(\sigma \rightarrow \sigma^*)$	$\Delta E_{NCT}(\sigma \rightarrow \sigma)$	$\Delta E_{CT}(\sigma_A \rightarrow \sigma_B^*)$	$\Delta E_{CT}(\sigma_B \rightarrow \sigma_A^*)$	$\Delta E_{CT}(\sigma_A \rightarrow \sigma_B)$	$\Delta E_{RP}(\sigma_A \rightarrow \sigma_A^*)$	$\Delta E_{RP}(\sigma_B \rightarrow \sigma_B^*)$
[CH ₂ CH ₂ ···OH]	0.015515	-0.186600	0.202115	-0.049155	-0.036036	-0.081135	-0.112108	-0.009393
[CH ₂ CHF···OH]	0.018045	-0.290560	0.308605	-0.053161	-0.034280	-0.082188	-0.204216	-0.008892
[CHFCH ₂ ···OH]	0.017006	-0.272023	0.289030	-0.051601	-0.037585	-0.085276	-0.205607	-0.009360
[CH ₂ CHCl···OH]	0.021962	-0.293256	0.315230	-0.057809	-0.041754	-0.093842	-0.194999	-0.000005
[CHClCH ₂ ···OH]	0.015054	-0.261244	0.276298	-0.046534	-0.037926	-0.081176	-0.179313	-0.007891

^a ΔE , barrier height; $\Delta E_{CT}(\sigma \rightarrow \sigma^*) - \Delta E_{\sigma\sigma^*}$; $\Delta E_{NCT}(\sigma \rightarrow \sigma) - \Delta E_{\sigma\sigma}$; $\Delta E_{CT}(\sigma_A \rightarrow \sigma_B^*)$, energy of delocalization from unit A to B estimated by deletion of appropriate Fock matrix elements; $\Delta E_{CT}(\sigma_B \rightarrow \sigma_A^*)$, energy of delocalization from unit B to A estimated by deletion of appropriate Fock matrix elements; ΔE_{RP} , repolarization energy within each unit.

Results of this study show that MP2 is the method of choice for the investigation of OH radical addition to double bonds if fairly large basis sets are used, starting from Pople's 6-311+G(3df,2p) and Dunning's aug-cc-pVDZ basis sets. Since satisfactory agreement with experimental results is obtained at the MP2/6-311+G(2d,p) level of theory, this can be used quite confidently to study reactions of larger unsaturated hydrocarbons and their mono- and polyhalogenated analogues that are of interest in environmental chemistry. In this way reliable estimates of their atmospheric lifetimes, and therefore their impact on ozone destruction and global warming, can be given. Since all the calculated barrier heights are too high, atmospheric lifetimes of the environmentally interesting unsaturated hydrocarbons should always be shorter than the predicted ones.

Barrier heights calculated at the B3LYP/6-311+G(2d,p) level are all too low, in agreement with previous investigations.³⁸ Also, reactivities are reversed with respect to experimental values. For example, a zero-point-corrected reaction barrier of $-2.9 \text{ kcal mol}^{-1}$ is predicted for the reaction of ethene with the OH radical. For the fluoroethene reaction both α - and β -additions have the same reaction barriers of $-3.5 \text{ kcal mol}^{-1}$. Results are somewhat better for the chloroethene reaction with the OH radical. The barriers are predicted to be -2.1 and $-1.5 \text{ kcal mol}^{-1}$ for α - and β -addition, respectively. Reaction enthalpies are also unexpectedly too low; for example, the measured value for ΔH_r in OH radical addition to ethene is -30.7 and the calculated value is $-25.5 \text{ kcal mol}^{-1}$. All results are summarized in Table 10.

C. Electronic Features and Reactivity. 1. *Enthalpies of Formation of Radical Products.* Calculated reaction enthalpies were used together with enthalpies of formation of haloalkenes and of the OH radical to estimate the enthalpies of formation of radical products formed in reactions R1, R2, and R3. The reaction enthalpies calculated at the MP2/aug-cc-pVTZ level were used in this procedure. The measured heat of formation for ethene²⁷ is $12.6 \text{ kcal mol}^{-1}$, for fluoroethene²⁷ $-33.2 \text{ kcal mol}^{-1}$, for chloroethene $3.5 \text{ kcal mol}^{-1}$, and for the OH radical $9.4 \text{ kcal mol}^{-1}$. The estimated enthalpies of formation are as follows: $\Delta H_f(\text{CH}_2\text{CH}_2\text{OH}) = -9.7 \text{ kcal mol}^{-1}$, $\Delta H_f(\text{CH}_2\text{-CHF}\text{OH}) = -63.4 \text{ kcal mol}^{-1}$, $\Delta H_f(\text{CHFCH}_2\text{OH}) = -53.9 \text{ kcal mol}^{-1}$, $\Delta H_f(\text{CH}_2\text{CHClOH}) = -23.0 \text{ kcal mol}^{-1}$, $\Delta H_f(\text{CHClCH}_2\text{-OH}) = -22.3 \text{ kcal mol}^{-1}$. The calculated enthalpies of formation for CH₂CH₂OH and CH₂CHClOH are in good agreement with the values determined from the group additivity model of -10.2 and $-23.7 \text{ kcal mol}^{-1}$ described in the Methods section. Somewhat larger discrepancies are obtained for $\Delta H_f(\text{CH}_2\text{CHFOH})$ since a value of $-57.9 \text{ kcal mol}^{-1}$ is obtained by the group additivity model. Predicted enthalpies of formation for the β -radicals are -53.9 and $-22.3 \text{ kcal mol}^{-1}$ for the CHFCH₂OH and CHClCH₂OH radicals, respectively.

2. *NBO Analysis of Reactants, Products, van der Waals Complexes, and Transition-State Structures.* Interactions of the OH radical with ethene and haloethenes in prereaction van der

Waals complexes, transition-state structures, and radical products were analyzed within the framework of the NBO method. Semiquantitative analysis of donor-acceptor interactions has been performed using second-order perturbation theory. Stabilization energy between bonding (σ) and antibonding (σ^*) NBOs, $\Delta E_{\sigma\sigma^*}^{(2)}$ is defined by eq 1. Since the systems studied are all open-shell, there are two different sets of natural bond orbitals $\{\sigma_{AB}\}$ and $\{\sigma_{AB}^*\}$. This approach is called *different hybrids for different spins*.²¹ The α spin system is called "filled" and has the Lewis structure that resembles an anion, while the β spin system is called "ionized" and has the Lewis structure that resembles a cation with the radical orbital formally empty.

In the transition-state structures the radical center is placed on the oxygen atom and is characterized by the oxygen nonbonding (lone-pair) orbitals in both spin sets. The orbital is occupied in the α spin system and almost unoccupied in the β spin system. Each spin system is well-described by a single Lewis structure. The most important delocalizations are given in Table 13 with corresponding delocalization energies, $\Delta E_{\sigma\sigma^*}^{(2)}$. In transition-state structures electron density delocalizations between $\sigma(C_1C_2) \rightarrow n^*(O)$ are significantly larger than $n(O) \rightarrow \sigma^*(C_1C_2)$ delocalizations. Therefore, we conclude that the OH radical acts as an electrophile in all investigated reactions. The largest $\sigma(C_1C_2) \rightarrow n^*(O)$ delocalization is calculated for the [CHClCH₂···OH] transition-state structure in agreement with the largest measured reactivity. The transformation from double to single C-C bond is stabilized by the halogen electron density donations, and it is largest for [CH₂-CHF···OH] transition-state structure. It is generally larger for fluoroethene transition-state structures than for chloroethene ones, as expected since fluorine is known to have a larger resonance effect on the π systems than chlorine.³⁹

In van der Waals prereaction complexes there is a weak delocalization of the electron density between the alkene double bond and the OH radical. The calculated $\Delta E_{\sigma\sigma^*}^{(2)}$ for $\sigma(C_1C_2) \rightarrow \sigma^*(HO)$ is $3.3 \text{ kcal mol}^{-1}$ for reaction R1, $2.5 \text{ kcal mol}^{-1}$ for reaction R2, and $1.7 \text{ kcal mol}^{-1}$ for reaction R3, in agreement with corresponding stabilization energies given in Table 12.

The radical product stabilities, e.g. reaction enthalpies, were also analyzed in terms of the NBO method. There is a positive correlation between reaction exothermicity and the strength of the newly formed C-O bond. The stability of the radical products is a very important factor that determines regioselectivity of addition reactions. This will be discussed in the next section. For the α -addition reaction of the OH radical to fluoroethene the C-O bond is additionally stabilized with electron density delocalized from halogen atom (Table 13). When the OH radical is added to the β -carbon there is no such stabilization of the C-O bond and β -addition reactions are less exothermic than the α -additions. In the case of β -additions, the radical center is stabilized by the transfer of electron density from the halogen atom, $n(\text{Hal}) \rightarrow n^*(C_2)$. According to such

an analysis, the following stability of the radical products can be predicted: $\text{CH}_2\text{CHFOH} > \text{CH}_2\text{CHClOH} > \text{CHClCH}_2\text{OH} > \text{CHFCH}_2\text{OH}$, in agreement with calculated reaction enthalpies and radicals' heat of formation. The larger stability of α -radicals in comparison to the β -radicals can be explained, in terms of frontier orbital approach, by antibonding contributions of the halogen atoms to the HOMO of the β -radical. In the HOMO of the α -haloradicals there are no such destabilizations, as shown in Figure 3b.

As described earlier (eq 1), the barrier heights for studied reactions can be decomposed into two terms, $\Delta E_{\sigma\sigma}$ and $\Delta E_{\sigma\sigma^*}$. Although the "UMP barrier heights" differ significantly from UHF values, indicating the important role of electron correlation effects; the qualitative conclusions drawn from the UHF results on the role of charge transfer are still valid.⁴⁰ The $\Delta E_{\sigma\sigma}$ term includes all the dominant effects of the steric repulsion between doubly occupied orbitals, electrostatic interactions between permanent dipole moments, etc. The $\Delta E_{\sigma\sigma^*}$ term describes donor-acceptor interactions (i.e., charge-transfer delocalizations). Two effects are included in $\Delta E_{\sigma\sigma^*}$: the repolarization within each reactant unit due to the other reactant unit and the charge transfer between reacting units.^{21b} These effects are separated by zeroing corresponding blocks of the Fock matrix in the NBO basis and recalculating the total energy. The energy associated with the charge transfer from OH radical to fluoroethene, $\Delta E_{\text{CT}}(\text{OH}^* \rightarrow \text{C}_2\text{H}_3\text{F})$, is found by zeroing the Fock matrix blocks connecting the σ orbitals of the OH radical (cores, lone pairs, and bonds) with the σ^* orbitals of fluoroethene (antibonds, Rydbergs). $\Delta E_{\text{CT}}(\text{C}_2\text{H}_3\text{F} \rightarrow \text{OH}^*)$ is found by zeroing the $\sigma(\text{C}_2\text{H}_3\text{F})-\sigma^*(\text{OH}^*)$ blocks. The repolarization energy ΔE_{RP} is found by zeroing the $\sigma-\sigma^*$ interactions within $\text{C}_2\text{H}_3\text{F}$ and OH units. All results are summarized in Table 13. The largest charge transfer between reacting units is predicted for the α -addition of the OH radical to chloroethene and the smallest for OH addition to ethene. Charge transfer allows a significant amount of exclusion repulsion to be overcome, like the repulsion between penetrating electron clouds and nuclear-nuclear repulsion, thus allowing the reacting units to approach each other more closely. This is consistent with the changes in the C-O distance, the shortest one for the $[\text{CH}_2\text{CHCl}\cdots\text{OH}]$ transition-state structure. However, the closer approach, enabled by the charge transfer between reaction units, increases in turn the electrostatic energy. Delocalization of electron density from the haloethene unit toward the OH radical is significantly larger than from the OH radical to the haloethene unit, in agreement with the calculated $\Delta E_{\sigma\sigma^*}^{(2)}$ values and proposed electrophilic character of the OH radical. The largest repolarization within each reactant unit is calculated for the fluoroethene moiety due to the resonance effect of the fluorine atom.

3. Reactivity and Regioselectivity of OH Radical Reactions with Ethene and Haloethenes. The calculated geometries of transition-state structures show very small changes in the olefinic C-C bond length (Table 2), but the calculated electronic properties of transition-state structures indicate very strong spin polarization on the carbon atoms (Table 14). Although spin polarization is not always an indicator of the bond-breaking process, it still indicates significant weakening of the olefinic double bond. Wiberg bond indexes⁴¹ were also calculated, and they are equal to 1.67 for $[\text{CH}_2\text{CH}_2\cdots\text{OH}]$, 1.64 for $[\text{CH}_2\text{-CHF}\cdots\text{OH}]$, 1.63 for $[\text{CHFCH}_2\cdots\text{OH}]$, 1.61 for $[\text{CH}_2\text{CHCl}\cdots\text{OH}]$, and 1.63 for $[\text{CHClCH}_2\cdots\text{OH}]$. Therefore, we conclude that the double-bond character of the olefinic bond is significantly smaller than expected from the geometric characteristics. Similar results were obtained for methyl radical addition to

TABLE 14: Atomic Spin Densities^a of van der Waals Complexes, Transition-State Structures, and Radical Products in Ethene, Fluoroethene, and Chloroethene Reactions with the OH Radical. The Numbering Scheme Is Given in Table 2

	$\rho^{\text{spin}}_{(r)}$		O
	C ₁	C ₂	
$[\text{CH}_2\text{CHX}\cdots\text{HO}]$			
X = H	-0.0008	-0.0010	1.0520
X = F	-0.0102	0.0099	1.0525
X = Cl	-0.0037	0.0018	1.0516
$[\text{CH}_2\text{CHX}\cdots\text{OH}]$			
X = H	0.7798	-0.6118	0.9029
X = F	0.7214	-0.5039	0.8927
X = Cl	0.7763	-0.5436	0.8820
$[\text{CHXCH}_2\cdots\text{OH}]$			
X = H			
X = F	-0.5928	0.7148	0.8966
X = Cl	-0.6041	0.7047	0.9109
CH_2CHXOH			
X = H	1.2698	-0.1621	0.0103
X = F	1.2721	-0.1275	0.0113
X = Cl	1.0969	-0.0536	0.0010
CHXCH_2OH			
X = H			
X = F	-0.0982	1.1228	0.0086
X = Cl	-0.0966	1.1227	0.0141

$$^a \rho_{(r)}^{\text{spin}} = \rho_{(r)}^{\alpha} - \rho_{(r)}^{\beta}$$

TABLE 15: Spin Densities^a of the $^3\pi\pi^*$ State and HOMO Coefficients for Ethene and Halogenated Ethenes. The Numbering Scheme for Atoms Is Given in Table 2

	$\rho_{(r)}^{\text{spin}}$		HOMO coefficients	
	C ₁	C ₂	C ₁	C ₂
ethene	0.6165	0.6165	0.6350	0.6350
fluoroethene	1.2914	1.0801	0.6426	0.5125
chloroethene	0.8685	0.3873	0.5620	0.4907

$$^a \rho_{(r)}^{\text{spin}} = \rho_{(r)}^{\alpha} - \rho_{(r)}^{\beta}$$

alkenes.^{7b} Halogen substitution decreases the length of the newly formed C-O bond, whereas it is longer in the case of β -addition than for α -addition. The same trend was observed for the radical products where the shorter and therefore stronger C-O bond is formed in α -addition reactions.

The main electronic interactions during free radical addition reactions to the double bond can be described as the spin density interactions between the radical and the alkene molecules. In the case of ethene, the triplet state $^3\pi\pi^*$ is described with one unpaired electron on each carbon atoms. Substitution of the halogen atom disturbs the symmetry of the electronic spin density and guides the reaction toward the place with larger spin density. Larger spin densities correspond usually to larger HOMO coefficients of the haloalkenes. Results for the fluoroethene and chloroethene are given in Table 15. In an orbital picture, the interaction can be considered as an interaction between π and π^* orbitals (HOMO and LUMO) and the SOMO orbital of the OH radical. In terms of UHF theory (where there are two, α and β , HOMO and LUMO orbitals), during the course of the reaction the radical center is shifted from the OH radical to the unattacked carbon atom of the haloalkene; that is the SOMO radical orbital is mixed with the α -HOMO orbital of the haloalkene. At the same time, β electron density is shifted in the opposite direction, i.e., to the newly formed C-O bond (Table 14). This process is illustrated in Figure 5, where the changes of the β -HOMO orbitals are shown along the reaction path. It easily can be seen that the new C-O bond is formed when critical accumulation of β electron density between

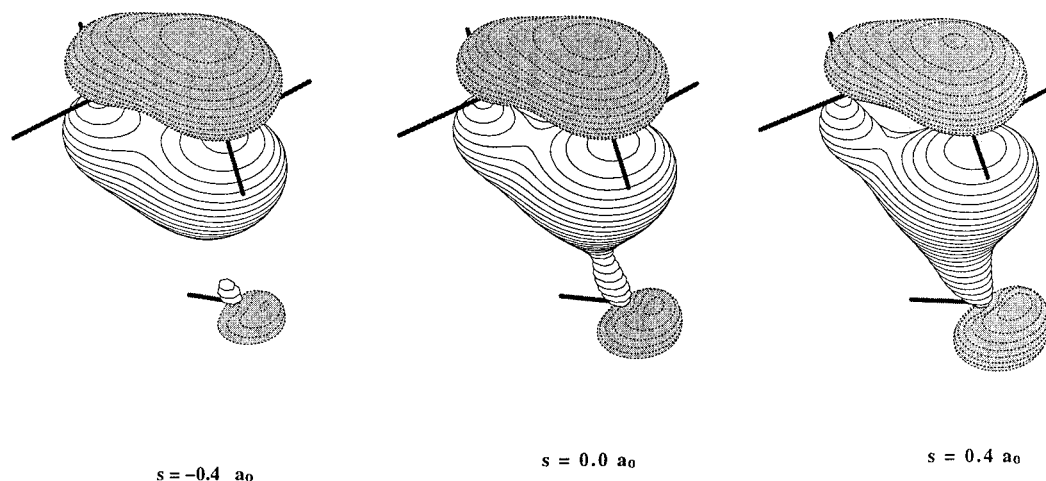


Figure 5. HOMO orbitals of the β spin set of transition-state structure ($s = 0.0 a_0$) and two structures along the reaction path ($s = \pm 0.4 a_0$).

reacting units is achieved. At the same time, β electron density is decreased on the neighboring carbon atom and α electron density is increased, respectively. Since, SOMO and HOMO orbitals are similar in energy, this interaction is the most important one at the beginning of the reaction. Therefore, in the case of haloethenes it can be expected that the OH radical addition to the unsubstituted carbon atom will be preferred. For the haloethene molecules, as already discussed earlier, the unsubstituted carbon atom has a larger HOMO coefficient since the halogen atom contributes in an antibonding fashion. The regioselectivity is in agreement with the calculated barrier heights for chloroethene reaction with the OH radical, but it is negligible in the case of fluoroethene. Furthermore, at all levels of theory used in this study α -addition is energetically favored with respect to β -addition (Table 9). Such results can be explained by two effects that influence regioselectivity of addition reactions. The first factor is the spin density in haloalkene molecules, which has been analyzed in terms of the SOMO–HOMO interaction. This factor directs the addition toward the carbon atom with larger spin density. The other factor is a thermodynamic one, namely, the strength of the C–O bond that is formed in the reaction. It favors the addition to the carbon atom that forms the stronger C–O bond. Regioselectivity is the net result of these two effects, and if they are synergistic, regioselectivity can be large, as in the case of vinylamine.⁴² In the case of fluoroethene, these two effects almost cancel each other, giving very similar barriers for α - and β -addition reactions. Chloroethene reaction with the OH radical is an example of a reaction where the thermodynamic effect is much smaller since reaction enthalpies for α - and β -addition are more similar than in the case of the fluoroethene reaction with the OH radical. Therefore, regioselectivity of the chloroethene reaction with the OH radical is dominated by SOMO–HOMO interaction and β -addition is favored because of the larger HOMO orbital coefficient.

Conclusions

The present study provides detailed insight into the hydroxyl radical reactions with ethene, fluoroethene, and chloroethene. Four stationary points were found along the MEP, and geometries were optimized and vibrational frequencies were calculated at the UMP2/6-311+G(2d,p) level of theory. Structures of prereaction complexes determined at the reactant side of the MEP are characterized by the weak interaction between the hydrogen atom of the OH radical and π electron density. Further along the MEP the OH bond is rotated toward the carbon

atom of the alkene and a new C–O bond is formed. In both prereaction complexes and transition-state structures the radical center still remains on the oxygen atom. The convergence of barrier heights and reaction enthalpies has been systematically investigated with respect to the size and quality of basis set and the treatment of correlation energy. The best agreement with experimental results is found at the MP2/aug-cc-pVTZ level of theory. The existence of the prereaction complexes was used to explain negative activation energies.

Regioselectivity is discussed in terms of two properties of the radical and the investigated alkenes. The first factor is the relative spin density of the $^3\pi\pi^*$ state of the alkene. The radical attack is directed toward the carbon atom with the highest spin density. The triplet density can be approximated with the HOMO density so that the largest HOMO coefficient corresponds to the highest triplet spin density. The second factor is the relative strengths of the product C–O bond, i.e., relative stability of the corresponding radical product. In the case of fluoroethene these two effects oppose each other and regioselectivity is negligible. In the case of chloroethene, spin density is the dominant factor and the addition to the unsubstituted carbon atom is preferred.

Acknowledgment. This work was supported by Grant 1-07-159 awarded by the Ministry of Science and Technology of the Republic of Croatia, by the U.S.-Croatian Science and Technology Joint Fund in cooperation with the U.S. Department of Agriculture and Croatian Ministry of Science and Technology under Project Number JF-120, and by the Forschungsförderungsfonds of Austria under Project Number P10404-PHY. This work was also carried out under the framework of the project “Fate and Activity Modelling of Environmental Pollutants using Structure–Activity Relationships (FAME)”, financially supported by the Environment and Climate Research and Technological Development Programme of the Commission of the European Union under Contract Number ENV4-CT96-0211 (DG 12-ESCY). Financial support from the European Union is gratefully acknowledged.

References and Notes

- (1) (a) *Combustion Chemistry*; Gardiner, W. C., Jr., Ed.; Springer: New York, 1984. (b) Hucknall, D. J. *Chemistry of Hydrocarbon Combustion*; Chapman and Hall: New York, 1985.
- (2) (a) Atkinson, R. *Chem. Rev. (Washington, D.C.)* **1986**, *86*, 69. (b) Atkinson, R. *J. Phys. Chem. Ref. Data* **1989**, Monograph 1. (c) Atkinson, R.; Baulch, D. L.; Cox, R. A.; Hampson, R. F., Jr.; Kerr, J. A.; Troe, J. J.

Phys. Chem. Ref. Data **1989**, 18, 881. (d) Atkinson, R. *J. Phys. Chem. Ref. Data* **1994**, Monograph 2.

(3) (a) Tuck, R.; Plumb, A.; Condon, E. *Geophys. Res. Lett.* **1990**, 17, 313. (b) Kerr, J. B.; *J. Geophys. Res.* **1991**, 96, 20703. (c) Stolarski, R.; Bojkov, R.; Bishop, L.; Zerefos, C.; Staehelin, J.; Zawodny, J. *Science* **1992**, 256, 342. (d) Kerr, R. A. *Science* **1993**, 262, 501. (e) Kerr, J. B.; McElroy, C. T. *Science* **1993**, 262, 1032. (f) Newman, A. *Environ. Sci. Technol.* **1993**, 27, 1488. (g) Rosswall, T. *Environ. Sci. Technol.* **1991**, 25, 567. (h) Ravishankara, A. R.; Turnipseed, A. A.; Jensen, N. R.; Barone, S.; Mills, M.; Howard, C. J.; Solomon, S. *Science* **1994**, 263, 71.

(4) (a) Barker, J. R. *Progress and Problems in Atmospheric Chemistry*; Advanced Series in Physical Chemistry Vol. 3; Baked, J. R., Ed.; World Scientific Publishing Co. Pte. Ltd.: Singapore, 1995; p 1.

(5) (a) Manzer, L. *Science* **1990**, 249, 31. (b) Farman, J. D.; Gardiner, B. G.; Shanklin, J. D. *Nature* **1985**, 315, 207. (c) Solomon, S. *Nature* **1990**, 347, 6291. Prinn, R. G. *Nature* **1990**, 344, 47. (d) Fisher, D. A.; Hales, C. H.; Filkin, D. L.; Ko, M. K. W.; Sze, N. D.; Connell, P. S.; Wuebbles, D. J.; Isaksen, I. S. A.; Stordal, F. *Nature* **1990**, 344, 508.

(6) (a) Mozurkewich, M.; Benson, S. W. *J. Phys. Chem.* **1984**, 88, 6429. (b) Chen, Y.; Tschuikow-Roux, E.; Raue, A. *J. Phys. Chem.* **1991**, 95, 9832. (c) Benson, S. W.; *Thermochemical Kinetics*; Wiley&Sons: New York, 1976; p 15.

(7) (a) Schlegel, H. B.; Sosa, C. *J. Phys. Chem.* **1984**, 88, 1141. (b) Canadell, E.; Eisenstein, O.; Ohanessian, G.; Poblet, J. M. *J. Phys. Chem.* **1985**, 89, 4856. (c) Delbecq, F.; Ilavsky, D.; Anh, N. T.; Lefour, J. M. *J. Am. Chem. Soc.* **1985**, 107, 1623. (d) Arnaud, R.; Subra, R.; Barone, V.; Leij, F.; Olivella, S.; Sole, A.; Russo, N. *J. Chem. Soc., Perkin Trans. 2* **1986**, 1517. (e) Clark, T. *J. Chem. Soc., Chem. Commun.* **1986**, 1774. (f) Arnaud, R. *New. J. Chem.* **1989**, 13, 543. (g) Zipse, H.; He, J.; Houk, K. N.; Giese, B. *J. Am. Chem. Soc.* **1991**, 113, 4324. (h) Tozer, D. J.; Andrews, J. S.; Amos, R. D.; Handy, N. C. *Chem. Phys. Lett.* **1992**, 199, 229. (i) Schmidt, C.; Warken, M.; Handy, N. C. *Chem. Phys. Lett.* **1993**, 211, 272. (j) Arnaud, R.; Vidal, S. *New. J. Chem.* **1992**, 16, 471. (k) Wong, M. W.; Pross, A.; Radom, L. *J. Am. Chem. Soc.* **1993**, 115, 11050. (l) Wong, M. W.; Pross, A.; Radom, L. *Isr. J. Chem.* **1993**, 33, 415. (m) Wong, M. W.; Pross, A.; Radom, L. *J. Am. Chem. Soc.* **1994**, 116, 6284. (n) Wong, M. W.; Pross, A.; Radom, L. *J. Am. Chem. Soc.* **1994**, 116, 11938. (o) Sosa, C.; Schlegel, H. B. *Int. J. Quantum Chem.* **1986**, 29, 1001. (p) Gonzalez, C.; Sosa, C.; Schlegel, H. B. *J. Phys. Chem.* **1989**, 93, 2435. (q) Houk, K. N.; Paddon-Row, M. N.; Spellmeyer, D. C.; Rondan, N. G.; Nagase, S. *J. Org. Chem.* **1986**, 51, 2874.

(8) (a) Tedder, J. M.; Walton, J. C. *Tetrahedron* **1980**, 36, 701. (b) Tedder, J. M. *Angew. Chem., Int. Ed. Engl.* **1982**, 21, 401. (c) Giese, B. *Angew. Chem., Int. Ed. Engl.* **1983**, 22, 753.

(9) (a) Sosa, C.; Schlegel, H. B. *J. Am. Chem. Soc.* **1987**, 109, 4193.

(b) Sosa, C.; Schlegel, H. B. *J. Am. Chem. Soc.* **1987**, 109, 7007.

(10) Donovan, W. H.; Famini, G. R. *J. Phys. Chem.* **1994**, 98, 7811.

(11) (a) Hehre, W. J.; Radom, L.; Schleyer, P. v. R.; Pople, J. *Ab Initio Molecular Orbital Theory*; Wiley-Interscience: New York, 1986. (b) Szabo, A.; Ostlund, N. S. *Modern Quantum Chemistry*; McGraw-Hill, Inc.: New York, 1982.

(12) Gonzalez, C.; Schlegel, H. B. *J. Phys. Chem.* **1990**, 94, 5523.

(13) Schlegel, H. B. *J. Phys. Chem.* **1988**, 92, 3075.

(14) Scott, A. P.; Radom, L. *J. Phys. Chem.* **1996**, 100, 16502.

(15) (15) (a) Pople, J. A.; Head-Gordon, M.; Fox, D. J.; Curtiss, L. A. *J. Chem. Phys.* **1989**, 90, 5622. (b) Curtiss, L. A.; Raghavachari, K.; Trucks, G. W.; Pople, J. A. *J. Chem. Phys.* **1991**, 94, 7221.

(16) (a) Dunning, T. H. *J. Chem. Phys.* **1989**, 90, 1007. (b) Kendall, R. A.; Dunning, Jr., T. H.; Harrison, R. J. *J. Chem. Phys.* **1992**, 96, 6796.

(17) Becke, A. D. *J. Chem. Phys.* **1993**, 98, 5648.

(18) (a) Lee, C.; Yang, W.; Paar, R. G. *Phys. Rev. B* **1988**, 37, 785. (b) Miehlich, B.; Savin, A.; Stoll, H.; Preuss, H. *Chem. Phys. Lett.* **1989**, 157, 200.

(19) Frisch, A. M. J.; Trucks, G. W.; Schlegel, H. B.; Gill, P. M. W.; Johnson, B. G.; Robb, M. A.; Cheesman, J. R.; Keith, T. A.; Petersson, G.

A.; Montgomery, J. A.; Raghavachari, K.; Al-Laham, M. A.; Zakrzewski, V. G.; Ortiz, J. V.; Foresman, J. B.; Cioslowski, J.; Stefanov, B. B.; Nanayakkara, A.; Challacombe, M.; Peng, C. Y.; Ayala, P. Y.; Chen, W.; Wong, M. W.; Andres, J. L.; Replogle, E. S.; Gomperts, R.; Martin, R. L.; Fox, D. J.; Binkley, J. S.; Defrees, D. J.; Baker, J.; Stewart, J. P.; Head-Gordon, M.; Gonzalez, C.; Pople, J. A. *Gaussian 94, Revision C.2.*; Gaussian, Inc.: Pittsburgh, PA, 1995.

(20) Glendening, E. D.; Reed, A. E.; Carpenter, J. E.; Weinhold, F. *NBO Program, Version 3.1.*

(21) (a) Foster, P.; Weinhold, F. *J. Am. Chem. Soc.* **1980**, 102, 7211.

(b) Reed, A. E.; Weinhold, F. *J. Chem. Phys.* **1983**, 78, 4066. (c) Reed, A. E.; Wehstock, R. B.; Weinhold, F. *J. Chem. Phys.* **1985**, 83, 735. (d) Reed, A. E.; Weinhold, F. *J. Chem. Phys.* **1985**, 83, 1736. (e) Reed, A. E.; Curtiss, L. A.; Weinhold, F. *Chem. Rev. (Washington, D.C.)* **1988**, 88, 899.

(22) Curtiss, L. A.; Pochatko, D. J.; Reed, A. E.; Weinhold, F. *J. Chem. Phys.* **1983**, 82, 2679.

(23) Tyrell, J.; Wehstock, R. B.; Weinhold, F. *Int. J. Quant. Chem.* **1981**, 19, 781.

(24) Carpenter, J. E.; Weinhold, F. *J. Mol. Struct.* **1988**, 169, 41.

(25) Diau, E. W.-G.; Lee, Y.-P. *J. Chem. Phys.* **1992**, 96, 377.

(26) *CRC Handbook of Chemistry and Physics*, 74th ed.; Weast, R. C., Astle, M. J., Beyer W. H., Eds.; CRC Press: Boca Raton, FL, 1993–1994. (27) Baulch, B. L.; Cox, R. A.; Hampson, R. F., Jr.; Kerr, J. A.; Troe, J.; Watson, R. T. *J. Phys. Chem. Ref. Data* **1984**, 13, 1376.

(28) (a) Sekušak, S.; Liedl, K. R.; Rode, B. M.; Sabljic, A. *J. Phys. Chem. A* **1997**, 101, 4245. (b) Sekušak, S.; Sabljic, A. *Chem. Phys. Lett.*, **1997**, 272, 353.

(29) Harmony, M. D.; Kuczowski, R. L.; Schwedeman, R. H.; Ramsay, D. A.; Lovas, F. J.; Lafferty, F. W. J.; Maki, A. G. *J. Phys. Chem. Ref. Data* **1979**, 8, 617.

(30) Harmony, M. D. *J. Chem. Phys.* **1990**, 93, 7522.

(31) Scott, A. P.; Radom, L. *J. Phys. Chem.* **1996**, 100, 16502.

(32) (a) Herzberg, G. *Molecular Spectra and Molecular Structure. II. Infrared and Raman Spectra of Polyatomic Molecules*; D. van Nostrand Company, Inc.: Toronto, 1968. (b) Bak, B.; Christensen, D. *Spectrochim. Acta* **1958**, 12, 355. (c) Gullikson, C. W.; Rud Nielsen, J. *J. Mol. Spectrosc.* **1957**, 1, 158.

(33) (a) Sekušak, S.; Güsten, H.; Sabljic, A. *J. Chem. Phys.* **1995**, 102, 7504. (b) Sekušak, S.; Güsten, H.; Sabljic, A. *J. Phys. Chem.* **1996**, 100, 6212. (c) Sekušak, S.; Güsten, H.; Sabljic, A. *J. Phys. Chem. A* **1997**, 101, 967 (correction). (d) Sekušak, S.; Sabljic, A. *J. Comput. Chem.* **1997**, 18, 1190.

(34) (a) Szczesniak, M. M.; Scheiner, S. *J. Chem. Phys.* **1986**, 84, 6328. (b) Yang, J.-a.; Kestner, N. R. *J. Phys. Chem.* **1991**, 95, 9214. (c) Wells, B. H.; Wilson, S. *Mol. Phys.* **1983**, 1983, 1295. (d) Gutowski, M.; van Lenthe, J. H.; Verbeek, J. H.; van Duijneveldt, F. B.; Chalasinski, G. *Chem. Phys. Lett.* **1986**, 124, 370. (e) Hobza, P.; Schneider, B.; Carsky, P.; Zahradnik, R. *J. Mol. Struct.* **1986**, 138, 377.

(35) Peterson, K. A.; Dunning, T. H., Jr. *J. Chem. Phys.* **1995**, 102, 2032.

(36) Feyereisen, M. W.; Feller, D.; Dixon, D. *J. Phys. Chem.* **1996**, 100, 2993.

(37) Liedl, K. R.; Sekušak, S.; Mayer, E. *J. Am. Chem. Soc.* **1997**, 119, 3782.

(38) (a) Dobbs, K. D.; Dixon, D. A. *J. Phys. Chem.* **1994**, 98, 12584. (b) Basch, H.; Hoz, S. *J. Phys. Chem. A* **1997**, 101, 4416. (c) Juršić, B. S. *J. Chem. Soc., Perkin Trans. 2* **1997**, 637. (d) Durant, J. L. *Chem. Phys. Lett.* **1996**, 256, 595.

(39) Pine, S. H.; Hendrickson, J. B.; Cram, D. J.; Hammond, G. S. *Organic Chemistry*, 4th ed.; McGraw-Hill, Inc: New York, 1980.

(40) (a) Reed, A. E.; Weinhold, F.; Curtiss, L. A.; Pochatko, D. J. *J. Chem. Phys.* **1986**, 84, 5687. (b) Hofmann, M.; Schleyer, P. v. R. *J. Am. Chem. Soc.* **1994**, 116, 4947.

(41) Wiberg, K. *Tetrahedron* **1968**, 24, 1083.

(42) Shaik, S. S.; Canadell, E. *J. Am. Chem. Soc.* **1990**, 112, 1446.